On the Mutual Coherence Function for Transionospheric Waves and its Utility for Characterizing Ionospheric Irregularities with a GNSS Scintillation Monitor

Charles S. Carrano, Charles L. Rino, Keith M. Groves, and Patricia H. Doherty
Institute for Scientific Research, Boston College, Boston, MA

BIOGRAPHY

Charles S. Carrano is a senior research physicist and Principal Investigator at Boston College's Institute for Scientific Research. He has authored and co-authored more than 40 technical papers concerning the impacts of ionospheric scintillation on radar, satellite communications, and Global Navigation Satellite Systems (GNSS). He is an Associate Editor of the AGU journal Radio Science, and serves on the Editorial Board of GPS Solutions. He has a B.S. degree from Cornell University and M.S. and Ph.D. degrees from The Pennsylvania State University.

Charles Rino is a visiting scholar at Boston College. He has worked in fields of electromagnetic wave paropagation and remote sensing for over 40 years. He was elected IEEE Fellow in 1989. He published *The Theory of Scintillation with Applications to Remote Sensing* in 2011. He has a Ph. D in Information and Computer Science from UC San Diego and MS and BSEE degrees from UC Berkeley.

Keith Groves works as a Senior Research Scientist at Boston College where his research interests include radio wave scintillations, high power HF ionospheric modification, wave-particle interactions, and space weather impacts on communication, navigation and surveillance systems. He has authored and co-authored more than 60 papers and is an internationally recognized expert in the field of ionospheric scintillations. He has a Ph.D. in Space Physics from MIT and a B.S. in Physics from Andrews University.

Patricia Doherty is Director of the Institute for Scientific Research at Boston College. She has been an active researcher in the area of radio wave propagation for the past 20 years, focusing on ionospheric effects on satellite-based navigation. She has led ionospheric research in support of Satellite-Based Augmentation Systems (SBAS), of which the FAA's Wide Area Augmentation System (WAAS) is an example. She has served in numerous volunteer offices in the Institute including the ION's Executive Committee and as program and general chair of the ION GNSS meeting. She is currently executive vice president of the Institute.

ABSTRACT

When interpreting GNSS observations of ionospheric scintillation, it is instructive to distinguish between the separate goals of characterizing the GNSS signal fluctuations and characterizing the disturbed ionospheric medium that produces the scintillations. The statistics of GNSS signal fluctuations are of primary interest for GNSS tracking loop analysis and design studies intended to quantify and model the impacts of ionospheric scintillation on navigation accuracy. Conversely, from an ionospheric physics standpoint, of primary interest are the statistical characteristics of the random ionospheric medium itself, and how these relate to the physical processes that structure the plasma. When the scintillation is weak, receiver diagnostics can serve both applications because the spectra of signal fluctuations at the ground are simply related to the spectra of variations in the ionospheric density.

On the other hand, when the scintillation is strong refraction and diffraction generate small scale structures in the fluctuating signal which have no counterparts in the ionosphere. Unraveling the characteristics of the ionospheric medium from strong signal fluctuations requires one to remove, or otherwise account for, these unwanted propagation effects. Sophisticated inverse techniques have been developed for this purpose. The Inverse Diffraction Method (Carrano et al., Proc. ION ITM, 2014) employs back-propagation to explicitly remove the unwanted propagation effects so that the statistics of the random ionospheric medium may be characterized directly. Another technique, called Iterative Parameter Estimation (Carrano et al., Int. J. Geophys., 2012), characterizes the random medium indirectly using nonlinear least-squares to fit the observations to numerical solutions of the differential equation governing the 4th moment of the fluctuating field. These techniques are relatively complex and can be quite computationally expensive (particularly the latter).

In this paper we explore an alternative approach that leverages the mutual coherence function (MCF) for transionospheric waves measured by a GNSS scintillation monitor to characterize the ionospheric disturbances that cause scintillation. For plane waves traversing a homogeneous random medium, the MCF is invariant to free-space propagation regardless of the scintillation strength. As such, fitting the MCF in the appropriate range of temporal separations can provide estimates for the strength and spectral index of electron density fluctuations that are largely uncorrupted by propagation effects (in essence, the statistics of an equivalent phase changing screen are inferred). This technique is simpler and computationally less demanding than the Inverse Diffraction Method or Iterative Parameter Estimation.

We demonstrate that fitting the MCF provides a more accurate description of the irregularities than measurements of T (phase spectral strength) and p (spectral index) provided by a GNSS scintillation monitor, since the latter may be corrupted by unwanted propagation effects. The approach we describe is relatively simple and suitable for implementation in the firmware of future GNSS scintillation monitors to provide improved ionospheric characterization in real time under both weak and strong scintillation conditions.

1. INTRODUCTION

Following Rino and Owen (1982), we define the mutual coherence function (MCF) for trans-ionospheric waves in terms of the complex amplitude u of the fluctuating radio wave evaluated at two points in the plane transverse to the propagating wave:

$$R_u(\boldsymbol{\rho},\boldsymbol{\rho}';z) = \left\langle u(\boldsymbol{\rho},z)u^*(\boldsymbol{\rho}',z)\right\rangle \qquad (1)$$

In the above, $\boldsymbol{\rho}$ and $\boldsymbol{\rho}$' represent position vectors in the transverse plane, and z is the coordinate along the propagation direction. In the above, '*' represents complex conjugation and <·> the ensemble average. Under the condition of narrow-angle scattering (which is amply satisfied for GNSS scintillations), it can be shown that the MCF satisfies the parabolic equation

$$\frac{\partial R_u}{\partial z} = -i\frac{k}{2}\left[\nabla_T^2 - \nabla_{T'}^2\right]R_u - \frac{1}{2}\frac{\partial D_{\delta\phi}(\boldsymbol{\rho},\boldsymbol{\rho}')}{\partial z}R_u \qquad (2)$$

where ∇_T is the transverse Laplacian operator and

$$D_{\delta\phi}(\boldsymbol{\rho},\boldsymbol{\rho}') = \left\langle\left[\delta\phi(\boldsymbol{\rho}) - \delta\phi(\boldsymbol{\rho}')\right]^2\right\rangle \qquad (3)$$

is the phase structure function. For the case of plane incident waves traversing a homogeneous medium the transverse Laplacian operators in (2) cancel and the equation can be solved, expressing the MCF in terms of the phase structure function:

$$R_u(\Delta\boldsymbol{\rho};z) = \exp\left\{-\tfrac{1}{2}D_{\delta\phi}(\Delta\boldsymbol{\rho})\right\} \qquad (4)$$

Thus the MCF is independent of the Fresnel parameter $\lambda z/4\pi$, and it is invariant during free-space propagation.

The purpose of this paper is to leverage this property of the MCF to provide estimates of the spectral index (p) and phase spectral strength (T) of the turbulent ionospheric medium that are uncorrupted by diffraction effects. Our approach is as follows. First,

we measure the MCF using observations of signal intensity and carrier phase scintillations, obtained either via simulation or from a GNSS scintillation monitor on the ground. Next we use equation (4) to infer the phase structure function of the random medium from the MCF. Lastly, we perform a least-squares fit using a model for the phase structure function to infer the strength and spectral index of the irregularities. We begin by presenting the model for the phase structure function that will be used to fit the data. The development follows that of Rino (1979) and Rino and Owen (1892).

We begin by assuming Rino's form for the power spectral density of phase fluctuations following oblique propagation through the disturbed ionospheric medium (Rino 1979)

$$\Phi_{\delta\phi}(\boldsymbol{\kappa}) = \frac{abC_p}{(\kappa_0^2 + A\kappa_x^2 + B\kappa_x\kappa_y + C\kappa_y^2)^{(p+1)/2}} \qquad (5)$$

where κ_x and κ_y are the transverse wavenumbers in the geomagnetic east and geomagnetic north directions. The turbulence is assumed to have outer scale L_0, and $\kappa_0=2\pi/L_0$ is the outer scale wavenumber. p is the phase spectral index. The scaling factors a and b elongate contours of constant phase correlation along and transverse to the magnetic field, respectively. The coefficients A, B, and C depend on the direction of propagation and the orientation of the irregularity axes. The parameter C_p is the strength of the 2D spatial spectrum of phase evaluated at the wavenumber 1 rad m^{-1}:

$$C_p = r_e^2 \lambda^2 C_s L \sec\theta . \qquad (6)$$

In the above, r_e is the classical electron radius (2.8179x10^{-15} m), λ is the wavelength, C_s is the strength of the 3D spatial spectrum of electron density fluctuations, L is the thickness of the scattering layer, and θ is the propagation (nadir) angle at the ionospheric penetration point (IPP).

The phase correlation function corresponding to this model spectrum is obtained by Fourier transformation of (5) and is given by (Rino, 1979):

$$R_{\delta\phi}(y) = GC_p \left|\frac{y}{2\kappa_0}\right|^{(p-1)/2} \frac{K_{\nu-1/2}(\kappa_0 y)}{2\pi\,\Gamma((\mathrm{p}+1)/2)} . \qquad (7)$$

Here $K_{\nu\text{-}1/2}$ is the modified Bessel function of order ν-1/2, and G is the geometric enhancement factor

$$G = \frac{ab}{\cos\theta\sqrt{AC - B^2/4}} \qquad (8)$$

The structure function of phase fluctuations, $D_{\delta\phi}$, can be expressed in terms of $R_{\delta\phi}$ as:

$$D_{\delta\phi}(y) = 2\left[R_{\delta\phi}(0) - R_{\delta\phi}(y)\right]. \qquad (9)$$

Evaluating (7) at zero separation is achieved by taking the limit y$\rightarrow$0. Assuming the random medium is invariant over the measurement interval, spatial fluctuations and temporal fluctuations are related by a model-dependent effective scan velocity. The effective scan velocity consistent with the Rino spectral model is (Rino, 1979)

$$V_{eff}^2 = \frac{CV_{sx}^2 - BV_{sx}V_{sy} + AV_{sy}^2}{AC - B^2/4} \qquad (10)$$

where V_{sx}, V_{sy} are the magnetic northward and eastward components of the plasma velocity relative to the scan velocity of the ray-path at the ionospheric penetration point (e.g. see Carrano et al, 2015). As first noted by Rino (1979), taking the Fourier transform of $R_{\delta\phi}(V_{\mathrm{eff}}\,\Delta t)$ gives the temporal spectrum of phase fluctuations in the absence of diffraction

$$\Phi_s(f) = \frac{T}{(f_0^2 + f^2)^{p/2}} \qquad (11)$$

where f is the temporal frequency of the time series, $f_0 = V_{\mathrm{eff}}/L_0$ is the outer scale frequency, and the phase spectral strength is

$$T = GC_p \frac{\Gamma(\frac{p}{2})}{4\pi^{3/2}\Gamma(\frac{p+1}{2})} V_{eff}^{p-1} . \qquad (12)$$

The parameters T and p provided by a GNSS scintillation monitor are computed by fitting the spectral density function (SDF) of phase fluctuations measured on the ground. These values will differ from (11) and (12) because of diffraction effects

which accumulate as the radio waves propagate down to the ground.

2. ESTIMATING IRREGULARITY PARAMETERS FROM SIMULATED DATA (VALIDATING THE METHOD)

To demonstrate the improvement in accuracy afforded by the current method, truth data is required for validation. For this reason, we begin by analyzing simulated scintillation data constructed via the multiple phase screen (MPS) method (Knepp, 1983; Carrano et al., 2011).

The details of these MPS simulations are as follows. A statistically homogenous layer of irregularities with thickness L=100 km centered at altitude 350 km was assumed. A series of 51 one-dimensional phase screens were distributed evenly throughout the layer spaced in altitude by approximately 2 km. Statistically independent realizations of phase in each screen were constructed from the spectral density function given by equations (11)-(12). We assumed nadir propagation through field-aligned irregularities at the magnetic dip equator, such that the geometrical phase enhancement factor is G=1. The effective scan velocity was taken to be V_{eff}=100 m/s. The outer scale was specified to be L_0 = 10 km, which corresponds to an outer temporal frequency of f_0= 0.01 Hz. The temporal sampling was 50 Hz and 2^{17} points were included in the screen. The total length of the screen time series was about 44 minutes. The phase spectral index p=2.5 was assumed. The phase spectral strength C_p was varied to produce the desired strength of scattering. The signal frequency was specified to be that of the GPS L1 carrier, namely 1575.42 MHz. The complex amplitude $u(t)$ of the wave after propagation through the 51 screens and then through free space down to the ground, forms the starting point for our analysis.

Of course, the method is ultimately intended to be used with real GNSS scintillation observations (examples will be provided in Section 4). In this case, the complex amplitude of the fluctuating wavefield at the receiver is computed from detrended normalized signal intensity (I_m) and detrended carrier phase (ϕ_m) measurements as:

$$u(t) = \sqrt{I_m(t)}\exp\left[i\phi_m(t)\right] \tag{13}$$

The phase detrending is performed to remove the geometric Doppler contribution due to satellite motion. A detailed description of the detrending procedure for intensity and carrier phase is provided in (Carrano et al., 2012).

Simulation #1 – A Weak Scatter Example

Figure 1 shows an example of the total screen phase, intensity fluctuations and phase fluctuations from the MPS simulation. Only the first 60 seconds of data are shown for the sake of clarity (the full time series was much longer, 44 min). The total screen phase is the sum of phase in each screen (i.e. the path integrated phase). Since the screens are uncorrelated, the sum of their individual variances is approximately equal to the variance of the total screen phase. A value of C_p=5.85×10^{-4} (SI units) was used to produce a weak scatter scenario with S_4=0.32 at the ground. The value of S_4 after traversing the last phase screen was 0.16, so that roughly half of the intensity disturbance developed inside the scattering layer. The intensity decorrelation time τ_I was 0.58 sec which, since the scatter is weak, is dictated by the effective scan velocity and Fresnel scale.

Note that the phase on the ground (Figure 1, bottom) is quite similar, but not identical, to the total screen phase (Figure 1, top). They are similar in this case because the scatter is weak. According to the weak scatter theory the spectrum of phase on the ground, $\Phi_p(K)$, is a filtered version of the screen spectrum, $\Phi s(K)$:

$$\Phi_p(K) = \Im(K,z,L,k)\,\Phi_s(K) \tag{14}$$

In (14) the spatial wavenumber K is related to the temporal frequency of the measured time series according to K=2$\pi f/V_{eff}$. In the Rytov approximation (weak scatter) the phase filter function is given by (Yeh and Liu, 1982):

$$\Im(K,z,L,k) = \frac{1}{2}\left[1+\frac{2k}{K^2L}\sin\left(\frac{K^2L}{2k}\right)\cos\left(\frac{K^2}{k}(z-L/2)\right)\right] \tag{15}$$

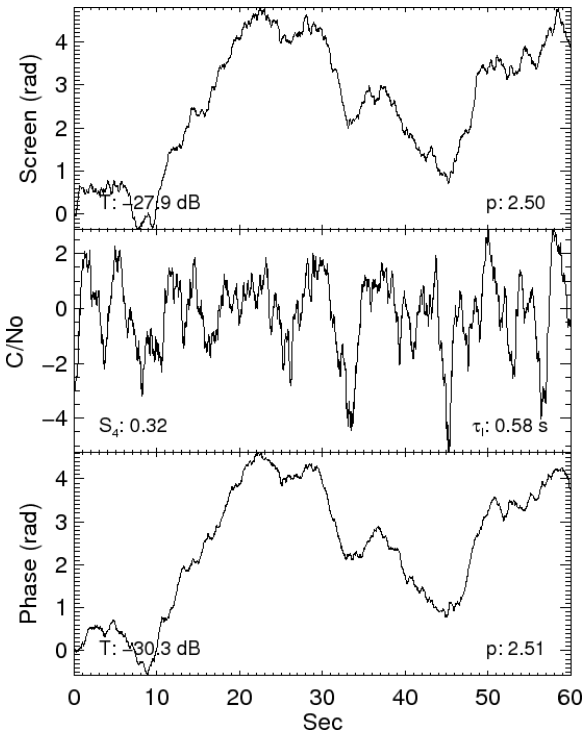

Figure 1. Weak scatter simulation results: total screen phase (top), and simulated intensity (middle) and phase (bottom) at the ground. The spectral strengths and slopes of the phases are shown on the plots, along with the S_4 index and intensity decorrelation time (τ_I).

The Rytov phase filter function at a distance of z = 350 km from the center of the scattering layer is shown in Figure 2. The solid line corresponds to an extended medium with L=100 km, while the dotted line corresponds to the limiting case $L \to 0$ (a thin phase screen). Note that the filter function oscillates about the average value 1/2 for large K. Also note that (14) and (15) imply the phase spectrum on the ground is strictly less than the spectrum of screen phase at all wavenumbers. As we shall see, a consequence of this filtering is that GNSS receivers that measure the fluctuation power by fitting the spectrum of phase fluctuations at the ground will underestimate the spectral power in the screen (by as much as a factor of 2) in weak scatter.

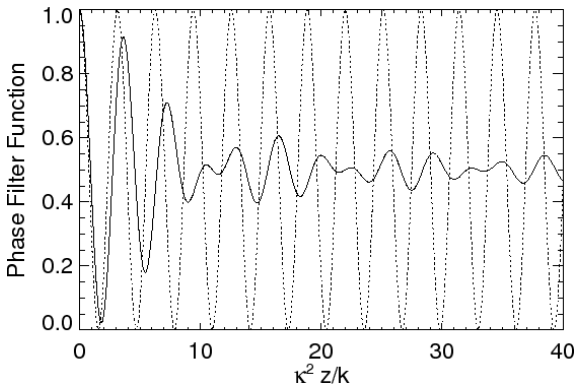

Figure 2. Phase filter function in the Rytov approximation (weak scatter). The solid line corresponds to an extended medium with L=100 km, the dotted line corresponds to a thin phase screen.

In this paper we compute spectral density functions using the Welch periodogram method (Welch, 1967). Each time series is divided into 32 subintervals for FFT analysis and then averaged with 50% overlap. The averaging is performed to minimize noise in the spectrum due to spectral leakage.

Figure 3 shows the spectral density functions of total screen phase (red), intensity fluctuations (green) and phase fluctuations (blue). Consistent with the weak scatter result (14) and (15), the spectra of ground phase and screen phase are nearly identical for frequencies smaller than the Fresnel break frequency $f_b = V_{eff}/(2z\sec\theta)^{1/2}$. The spectrum of ground phase is a roughly half as large as the spectrum of screen phase (on average) for frequencies significantly larger than the break frequency. By definition, the phase spectral power T is the value of (11) evaluated at 1 Hz (since the outer scale frequency is <<1 Hz). We measure T and p by performing a log-log linear least-squares fit to the spectra in the vicinity of f=1 Hz. Since f_b<<1 Hz in this case, the value of T obtained by fitting the phase spectrum (-30.32dB) is 43% smaller (in terms of linear units) than the value inferred from the screen (-27.89dB). This result is typical of weak scatter conditions, in that p can be accurately estimated from the ground phase but T is underestimated relative to the screen fluctuations. This situation, of course, will lead to an underestimate of the irregularity strength unless the diffraction effects are excluded from the analysis.

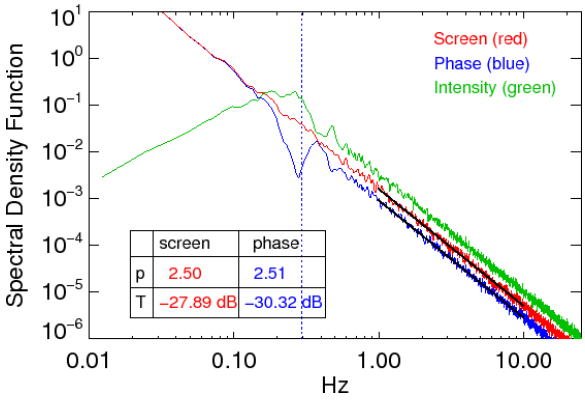

Figure 3. Spectral density functions of the total screen phase (red), and intensity (green) and phase (blue) at the ground for the data shown in Figure 1.

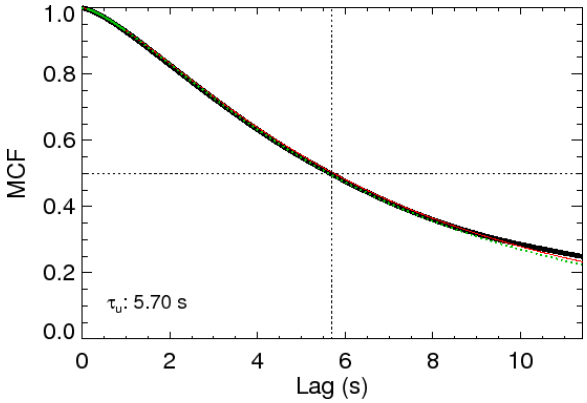

Figure 4. Mutual coherence function (black) computed from the intensity and phase measurements shown in Figure 1. The decorrelation time of the MCF is labeled. Also shown are the theoretical MCF (red) and the fitted MCF (green).

The purpose of this paper is to show how these diffraction effects may be mitigated to recover the statistics of screen phase from the scintillation measurements. The first step is to compute the Doppler spectrum by applying the FFT to $u(t)$ and multiplying the result by its complex conjugate. Following Rino and Owen (1982) we average the positive and negative frequency components of the Doppler spectrum to force it to be symmetrical about the DC component (f=0). The mutual coherence function is then computed by applying the inverse FFT to the symmetrized Doppler spectrum.

Figure 4 shows the MCF versus time lag τ derived from the intensity and phase measurements shown in Figure 1. The time lag to 50% decorrelation in this case was 5.70 sec. The theoretical MCF result, evaluated by computing the intermediate quantity $D_{\delta\phi}(V_{eff}\ \tau)$ from (7)-(10) and plugging this into (4), is over-plotted in red and agrees with the data very well (thus verifying the simulation). The quality of this agreement suggests that one may infer the statistical parameters of the screen by least-squares fitting the measured MCF with the theoretical model. While this is indeed a viable approach, Rino and Owen (1982) showed that the MCF itself is relatively insensitive to small changes in the high frequency content of the ionospheric structure (which is of particular interest). For this reason, we take a slightly different approach.

The approach we take is to use (4) to infer the structure function of screen phase from the measured MCF, i.e.

$$D_{\delta\phi}(\Delta\boldsymbol{\rho}) = -2\ln R_u(\Delta\boldsymbol{\rho}) \qquad (16)$$

and then fit the structure function with a model instead of the MCF itself. Throughout this paper, we will occasionally use the terminology "fitting the mutual coherence function," for simplicity, when in fact we are fitting the structure function of screen phase (or, equivalently, path integrated phase) derived from the MCF through equation (16).

Figure 5 shows the structure function of screen phase (black) versus time lag τ along with the theoretical curve $D_{\delta\phi}(V_{eff}\ \tau)$ (red). Also shown is the structure function computed from the phase measured at the ground (blue dashed curve). Note that the ground phase structure function is smaller than the screen phase structure function for all temporal separations. The reason for this is that the ground phase is a filtered version of the screen phase, according to equation (15).

Once the structure function of screen phase has been computed, we "pretend" not to know the screen parameters and estimate C_p and p by fitting the theoretical model $D_{\delta\phi}(V_{eff}\ \tau)$ to the phase structure function just computed. Once C_p and p are known, the screen spectral power T can be estimated (if

desired) using (12). Note that this requires knowledge of G and V_{eff}, which can be computed from the satellite motion, propagation geometry, and irregularity drift (Carrano et al., 2012b). We perform the least squares fitting in log-log space using the downhill simplex method (Nelder and Mead, 1965). This algorithm is relatively robust for nonlinear minimization problems and has the advantage that analytic gradients of the fitting function are not required. A close initial guess for the parameters to be determined is required, but this may be obtained by leveraging the approximate theoretical relationship between S_4 and C_sL described by Carrano et al. (2012b).

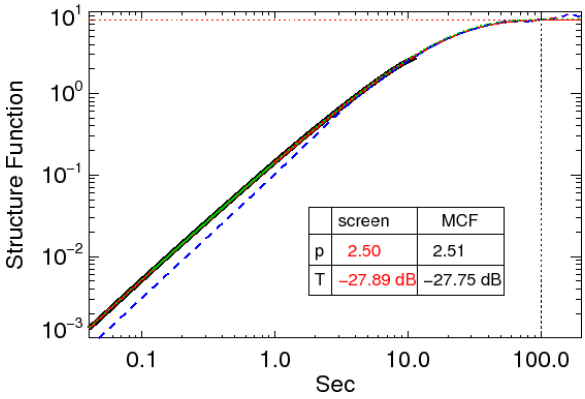

Figure 5. Phase structure function (black) derived from the MCF shown in Figure 4. Also shown are the theoretical (red) and fitted (green) phase structure functions. Shown for comparison is the structure function of phase fluctuations at the ground (blue dashed).

The values of T and p obtained by fitting the screen phase spectrum in the range 1-10Hz were -27.89 dB and 2.50, respectively. By fitting the structure function of screen phase obtained from the measured MCF (in the range 0.1-1.0 sec), we obtain estimates for T and p as -27.75 dB and 2.51, respectively. This least-squares fit to the structure function is shown in Figure 5 as the green curve; the MCF corresponding to this fit appears in Figure 4 as the green curve. There is excellent agreement between the parameters obtained by fitting the phase structure function and the known screen parameters, demonstrating that we have effectively mitigated the effects of diffraction and accurately recovered the statistical parameters describing the ionospheric irregularities from the scintillation measurements on the ground. More precisely stated, we have recovered the statistics of path-integrated phase, or an equivalent phase screen, from the observed scintillation data.

Simulation #2 – A Strong Scatter Example

Next we consider a strong scatter example. Figure 6 shows an example of the total screen phase, intensity fluctuations and phase fluctuations from the MPS simulation. A value of C_p=1.37×10^{-2} (SI units) was used to produce a strong scatter scenario with S_4=0.96. The value of S_4 after traversing the last phase screen was 0.66, so that the intensity disturbance developed significantly while inside the scattering layer. The intensity decorrelation time τ_I was 0.32 sec, which is much shorter than the corresponding value for the weak scatter case (Figure 1). This shortening is caused by multiple scatter effects (Carrano et al., 2010).

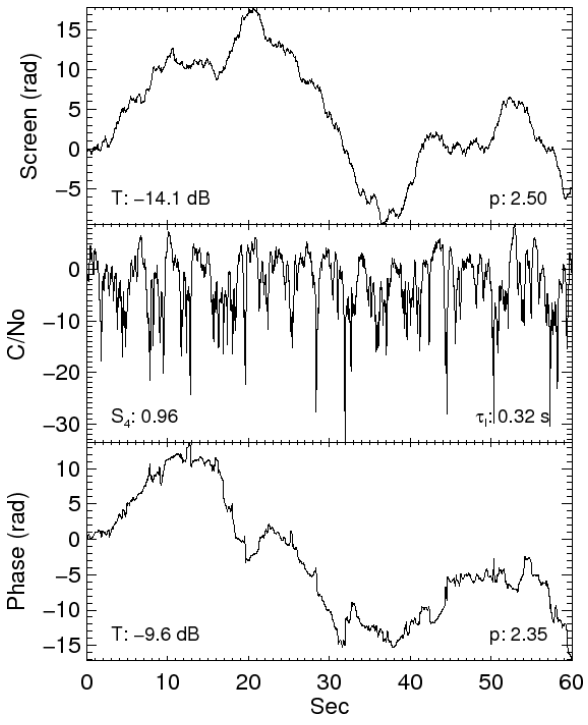

Figure 6. Strong scatter simulation results: total screen phase (top), and simulated intensity (middle) and phase (bottom) at the ground. The spectral strengths and slopes of the phases are shown on the plots, along with the S_4 index and intensity decorrelation time (τ_I).

Note that the ground phase exhibits rapid phase transitions at times corresponding to deep signal fades. These rapid phase transitions are not cycle slips (there are no cycle slips in a well-resolved phase screen simulation), instead they are a consequence of the complex amplitude wandering close to the origin in the complex plane where small movements can result in large phase accumulations. Each of these rapid transitions occurs over the span of multiple data samples, and is not a discontinuous event (Carrano et al., 2013). These rapid phase transitions create high frequency content in the measured phase that has no counterpart in the ionosphere. The presence of these rapid transitions also causes the large scale phase structure to depart significantly from that of the measured phase, as can been seen from Figure 6.

Figure 7 shows the spectral density functions of the screen (red), and intensity fluctuations (green) and phase fluctuations (blue). Unlike the weak scatter case (compare with Figure 3), the phase spectrum is much shallower than the screen spectrum. Moreover, the phase spectrum exceeds the screen spectrum at all frequencies. Whereas the screen phase power and spectral index are -14.15dB and 2.50, respectively, the power and spectral index obtained by fitting the spectrum of measured phase are -9.60 dB and 2.35, respectively. The measured phase fluctuations have 2.9 times larger fluctuation power than the ionospheric screen which produced them. Attempts to measure the irregularity spectral index using the phase will significantly underestimate the true value. All of these effects are caused by the rapid phase transitions due to diffraction which drive the measured phase spectrum to that of a discontinuous random process (which has a spectral index of 2).

Also unlike the weak scatter case (compare with Figure 3), the intensity spectrum has broadened significantly, departing from power law form at intermediate frequencies. This spectral broadening is a well-known manifestation of strong-scatter effects (Carrano et al., 2010; 2012a).

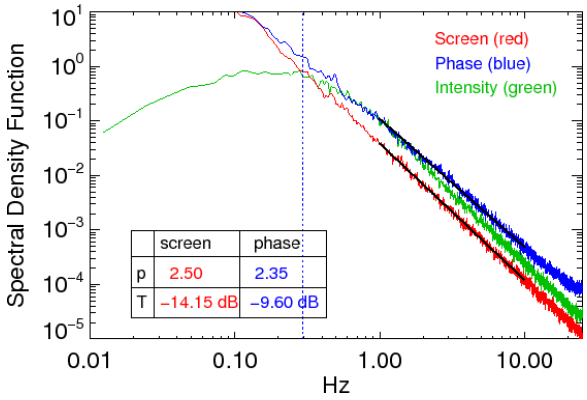

Figure 7. Spectral density functions of the total screen phase (red), and intensity (green) and phase (blue) at the ground for the data shown in Figure 6. The vertical dotted line indicates the Fresnel break frequency.

Despite the significant departures in the spectral content of intensity and phase fluctuations relative to the irregularities that caused them, we can mitigate the effects of diffraction and recover the screen phase following the same procedure as before. First, we compute the MCF using the measured complex amplitude (Figure 8). The theoretical MCF result is shown in red. As before, the theoretical MCF is evaluated by computing the intermediate quantity $D_{\delta\phi}(V_{eff}\ \tau)$ from (7)-(10) and plugging this into (4). The time lag to 50% decorrelation of the MCF is 0.54 sec in this case, which can be compared with 5.54 sec for the weak scatter case. This shortening is due to multiple scatter effects.

Next, we use equation (16) to infer the structure function of screen phase (Figure 9) from the measured MCF. Also shown in the figure is the structure function of measured phase (blue dashed curve), which is significantly larger than the screen structure function for all time lags. Equivalently stated, the ground phase has more fluctuation power at all frequencies than the screen phase. This discrepancy is also due to the rapid phase transitions caused by diffraction. The theoretical curve $D_{\delta\phi}(V_{eff}\ \tau)$ is shown in Figure 9 as the red curve, while the least-squares fit, in the range 0.1-1.0 sec, is shown as the green curve. The MCF corresponding to this fit is shown as the green curve in Figure 8.

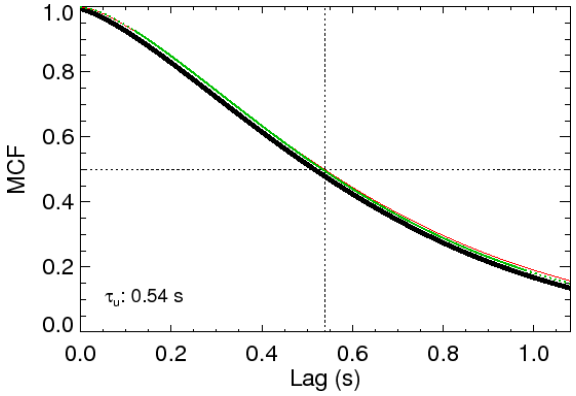

Figure 8. Mutual coherence function (black) computed from the intensity and phase measurements shown in Figure 6. The decorrelation time of the MCF is labeled. Also shown are the theoretical MCF (red) and the fitted MCF (green).

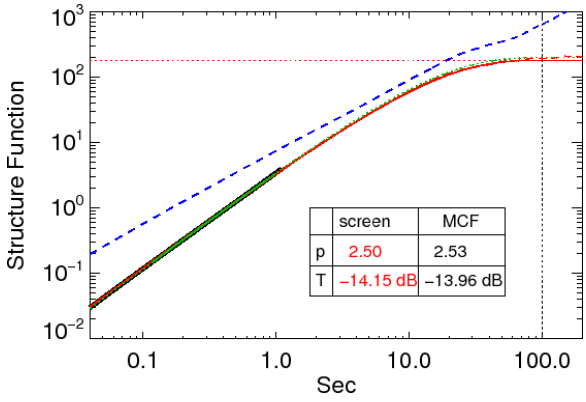

Figure 9. Phase structure function (black) derived from the MCF shown in Figure 8. Also shown are the theoretical (red) and fitted (green) phase structure functions. Shown for comparison is the structure function of phase fluctuations at the ground (blue dashed).

As before, given the structure function of screen phase, we can fit the theoretical model $D_{\delta\phi}(V_{eff}\ \tau)$ to determine the screen parameters C_p and p. Once these are known, the screen spectral power T can be computed using (12). The values of T and p obtained by fitting the screen SDF directly were -14.15dB and 2.50, respectively. By fitting the structure function of screen phase obtained from the measured MCF, we obtain estimates for T and p as -14.71 dB and 2.51, respectively. The agreement is excellent, even in this case of very strong scatter. Again we have successfully mitigated the effects of diffraction and accurately recovered the statistical parameters describing the ionospheric irregularities from the scintillation measurements on the ground.

3. ACCURACY OF IRREGULARITY PARAMETER ESTIMATES AS A FUNCTION OF IRREGULARITY STRENGTH

In the preceding section, we examined two simulation scenarios in detail, one weak scatter case with S_4=0.32 and one strong scatter case with S_4=0.96. For both cases we showed that diffraction effects could be mitigated and the screen parameters recovered by fitting the structure function of screen phase derived from the measured MCF. In this section we apply the technique to complex amplitude "measurements" provided by twenty MPS simulations with varying screen strengths. We compare estimates of T and p derived in this way with the known parameters of the screen. We also compare them with those inferred directly from the spectrum of measured phase fluctuations (as current GNSS scintillation monitors do).

All of the plots in this section use the same color coding scheme. The red curve shows the estimates inferred directly from a linear log-log fit of the screen spectrum. The blue curve shows the estimates inferred directly from a linear log-log fit of the spectrum of measured phase. The black curve shows the estimates inferred by least-squares fitting the structure function of screen phase derived from the measured MCF.

In Figure 10 we show the estimates of spectral index (p) plotted as a function of the value of screen spectral power (T). When the screen spectral power is less than -23 dB, all three estimates are essentially equivalent. That is to say, the spectral index of the irregularities can be accurately measured by fitting the spectrum of measured phase fluctuations, provided the scatter is weak. When the scatter is strong, diffraction effects cause shallower estimates of the spectral index to be obtained using the measured phase. Nevertheless, the true spectral index can be retrieved accurately for all levels of scatter by fitting the structure function of screen phase derived from the measured MCF.

In Figure 11 we show estimates of phase spectral power (T) plotted as a function of the value of screen spectral power (T). As before, the blue curve shows the estimates obtained via linear log-log fit of the spectrum of measured phase. The plot clearly shows that the screen spectral strength is underestimated (by approximately a factor of 2) in weak scatter, and overestimated (by up to a factor of 2.8) in strong scatter. The cross-over point between underestimating and overestimating the screen power occurs at T≈-23 dB. Comparing the red and black curves, the screen spectral power can be recovered almost perfectly at all levels of scatter by fitting the screen structure function derived from the MCF.

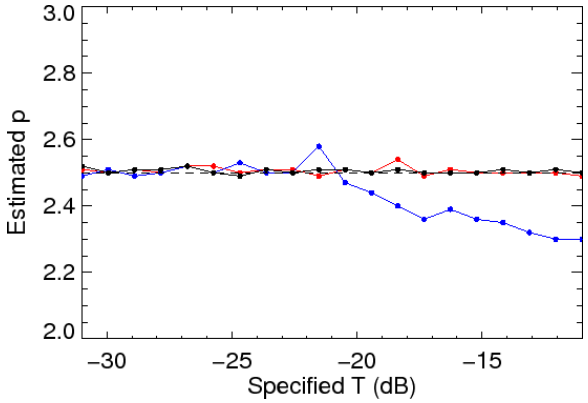

Figure 10. Estimated phase spectral index versus the specified spectral strength of the screen. The red, blue, and black points were estimated from the screen phase, ground phase, and structure function of screen phase derived from the MCF, respectively.

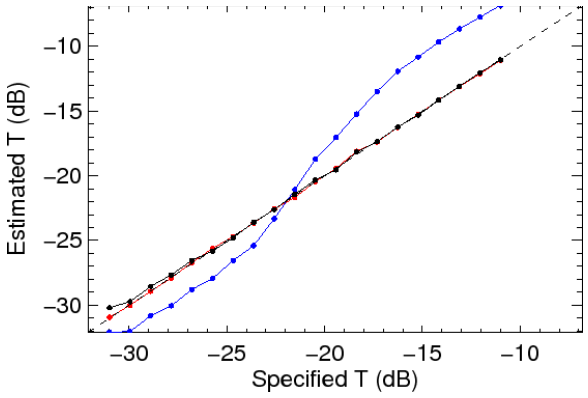

Figure 11. Estimated phase spectral strength versus the specified spectral strength of the screen. The red, blue, and black points were estimated from the screen phase, ground phase, and structure function derived from the MCF, respectively.

Figures 12 and 13 are similar to Figures 10 and 11, except that the strength of scatter is quantified in terms of S_4 rather than T. Figure 12 shows that the spectral index of the irregularities can be accurately measured by fitting the spectrum of measured phase fluctuations when S_4<0.6. When S_4 exceeds 0.6 this ceases to be true because the phase includes spurious high frequency content. Nevertheless, as the black curve shows, the true spectral index can be retrieved accurately for all levels of scatter by fitting the MCF. Figure 13 shows that the screen spectral strength is underestimated when S_4<0.6, and when S_4>0.6. The underestimates are a consequence of the phase filter function (15). The overestimates are due to the rapid phase transitions that occur in strong scatter.

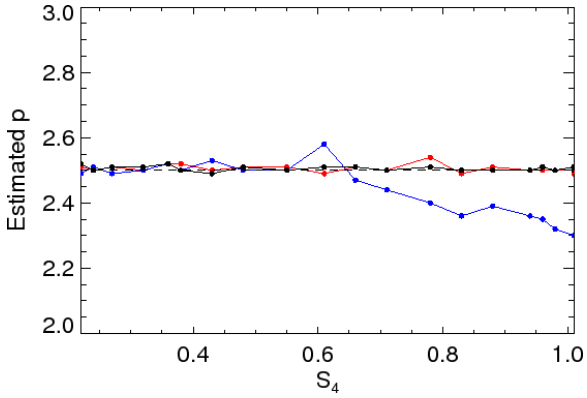

Figure 12. Estimated phase spectral index versus the S_4 index. The red, blue, and black points were estimated from the screen phase, ground phase, and structure function of screen phase derived from the MCF, respectively.

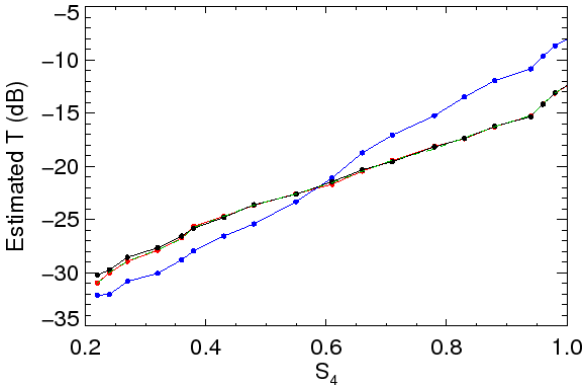

Figure 13. Estimated phase spectral strength versus the S_4 index. The red, blue, and black points were estimated from the screen phase, ground phase, and structure function of screen phase derived from the MCF, respectively.

4. ESTIMATING IRREGULARITY PARAMETERS FROM SCINTILLATION OBSERVATIONS

With funding and support from the Federal Aviation Administration (FAA), Boston College and National Institute for Space Research (INPE) in Brazil have collaborated to collect GPS scintillation observations on the L1, L2, and L5 carrier signals since April 2012. A Septentrio PolaRxS Pro GNSS receiver reports 50 Hz samples of post-correlator in-phase (I) and quadrature (Q) data, along with carrier phase measurements at the L1, L2, and L5 frequencies. This receiver is located at the INPE headquarters in São José dos Campos, Brazil (23.2°S, 45.9°W, 17.5°S dip latitude). São José is located near the southern crest of the equatorial anomaly, where the strongest scintillations tend to occur globally. The raw I&Q samples and carrier-phase measurements have been post-processed to obtain the normalized and detrended intensity and phase fluctuations due to ionospheric scintillation, using the methodology described in (Carrano et al., 2012).

In this section we apply the fitting procedure described in Section 2 to two scintillation observations at São José dos Campos on 29 November 2012. The first observation is an example of weak scatter conditions, while the second is an example of strong scatter conditions. The phase geometrical enhancement factor G and effective scan velocity V_{eff}, required for fitting the MCF, were calculated as described in [Carrano et al., 2014] using spaced UHF antenna measurements of the zonal irregularity drift from nearby Cuiaba, Brazil.

Observation #1 – A Weak Scatter Example

The normalized intensity and phase fluctuations observed at São José dos Campos for GPS PRN 29 are shown in Figure 14. The intensity fluctuations are small (a few dB) and the scattering is weak (S_4=0.27). The SDF of the phase fluctuations is shown in Figure 15, along with a log-log linear fit used to determine the phase spectral strength T=-40.7 dB and slope p=2.82. Since these are real observations, we cannot directly compare these values with those associated with the path integrated phase (i.e. in the absence of diffraction) as we did for the simulation examples in Section 2. In fact, it may be possible to perform such a comparison by inferring an equivalent phase screen via back-propagation [Carrano et al., 2014], but this exercise would be beyond the scope of this paper.

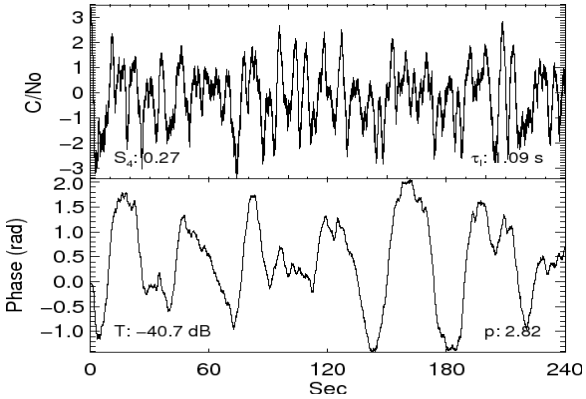

Figure 14. Weak scintillations of the GPS L1 signal from PRN 29 observed on 29 Nov 2012 starting at 01:32 UT: (top) normalized intensity fluctuations, and (bottom) phase fluctuations. The S_4 index and intensity decorrelation time (τ_I) are shown, along with the spectral strength and slope of the observed phase fluctuations.

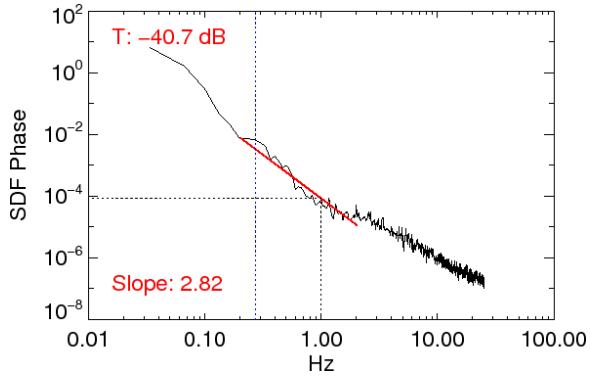

Figure 15. SDF of the phase fluctuations shown in Figure 14. Also shown (red) is a log-log linear fit to the SDF and corresponding phase spectral strength (T) and slope (p).

The mutual coherence function computed from these weak scintillation observations is shown in Figure 16. The decorrelation time of the MCF is 7.68 sec. Figure 17 shows the structure function of screen phase derived from the MCF. Also shown in Figure 17, for comparison, is the structure function computed from the measured phase fluctuations at the receiver (blue). Note that the ground phase has less fluctuation

power than the screen phase at all frequencies, as predicted by the weak scatter theory and in accord with the simulation results discussed in Section 2 (compare with Figure 5). The least-squares fit to the structure function and corresponding MCF are shown as green curves in Figures 17 and 16, respectively. From this fit we estimate the screen phase parameters T=-38.63 dB and p=2.95. While these estimates are reasonably close to those obtained directly from the measured phase fluctuations, we expect the former to be more accurate. The phase spectral strength estimated from the ground phase is, in fact, 40% smaller than that estimated by the fitting the MCF.

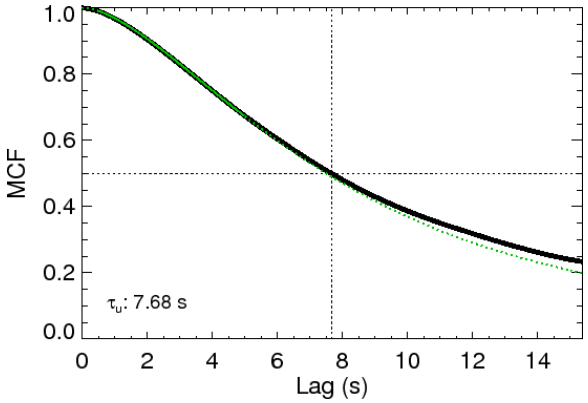

Figure 16. Mutual coherence function (black) computed from the intensity and phase measurements shown in Figure 14. The decorrelation time of the MCF is labeled. The fitted MCF is shown in green.

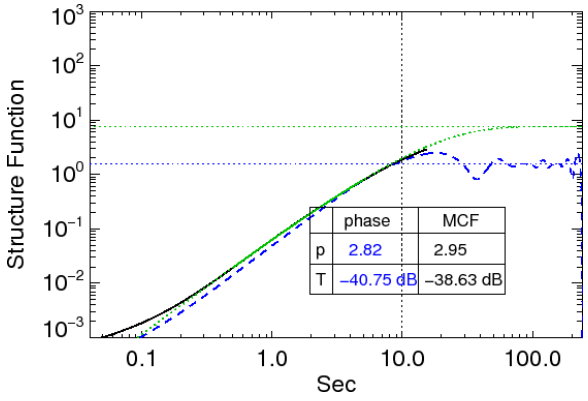

Figure 17. Structure function of screen phase (black) derived from the MCF shown in Figure 16. The fitted phase structure function is shown in green. Shown for comparison is the structure function of phase fluctuations at the ground (blue dashed).

Observation #2 – A Strong Scatter Example

Next, we consider a case of strong scintillation. Figure 18 shows the normalized intensity and phase fluctuations observed at São José dos Campos for GPS PRN 25. The intensity fluctuations are intense, with fades exceeding 30dB, and S_4 is saturated at unity. The phase fluctuations clearly exhibit rapid phase transitions caused by diffraction that coincide with the deep signal fades. These rapid transitions are not instantaneous cycle slips; instead they take place over many data samples. Their presence alters the spectrum of phase fluctuations that a GNSS scintillation monitor measures on the ground, compared with the spectrum of path integrated phase.

The spectral density function of the measured phase fluctuations is shown in Figure 19, along with a log-log linear fit used to determine the phase spectral strength T=-24.0 dB and slope p=2.30. These parameters are undoubtedly corrupted by diffraction effects, but since these are real observations we do not have access to the path integrated phase needed to quantitatively substantiate this assertion.

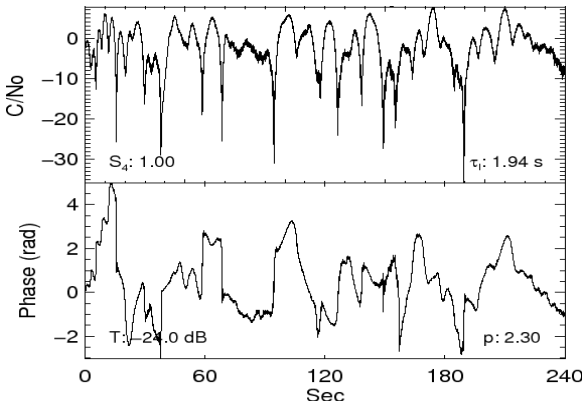

Figure 18. Strong scintillations of the GPS L1 signal from PRN 25 observed on 29 Nov 2012 starting at 02:14 UT: (top) normalized intensity fluctuations, and (bottom) phase fluctuations. The S_4 index and intensity decorrelation time (τ_I) are shown, along with the spectral strength and slope of the observed phase fluctuations.

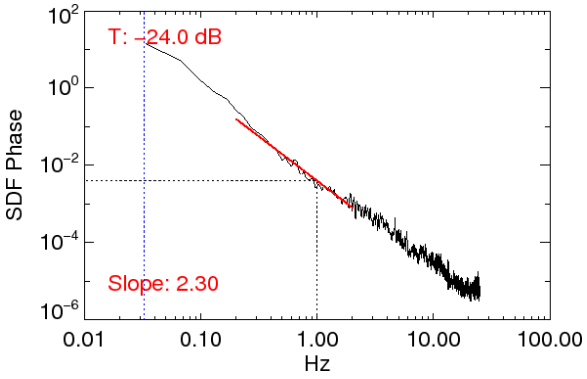

Figure 19. SDF of the phase fluctuations shown in Figure 18. Also shown (red) is a log-log linear fit to the SDF and corresponding phase spectral strength (T) and slope (p).

The mutual coherence function computed from these strong scintillation observations is shown in Figure 20. The decorrelation time of the MCF is 3.24 sec, which is significantly shorter than that for the weak scatter case (7.68 sec). This shortening is a consequence of multiple-scatter effects. Figure 21 shows the structure function of screen phase derived from the MCF. Also shown for comparison is the structure function computed from the phase fluctuations at the receiver (blue). Note that the ground phase has significantly more fluctuation power than the inferred screen phase at all frequencies, in accord with the simulation results described in Section 2 (compare with Figure 9). The least-squares fit to the structure function and corresponding MCF are shown as green curves in Figures 21 and 20, respectively. From this fit we estimate the screen parameters T=-24.05 dB and slope p=2.97. As expected, the spectral index obtained from the ground phase is significantly smaller than that obtained by fitting the structure function implied by the MCF. The presence of rapid transitions in the ground phase due to diffraction drives the spectral density function to that for a discontinuous random process (which has a spectral index of 2). Furthermore, the phase spectral strength estimated from the ground phase is about twice that estimated by the fitting the structure function implied by the MCF.

We noted very similar behavior for the strong scatter simulation case presented in Section 2. For this reason, we believe the technique of fitting the structure function implied by the MCF effectively mitigates the effects of diffraction and recovers the statistical parameters describing the ionospheric irregularities from the scintillation measurements on the ground.

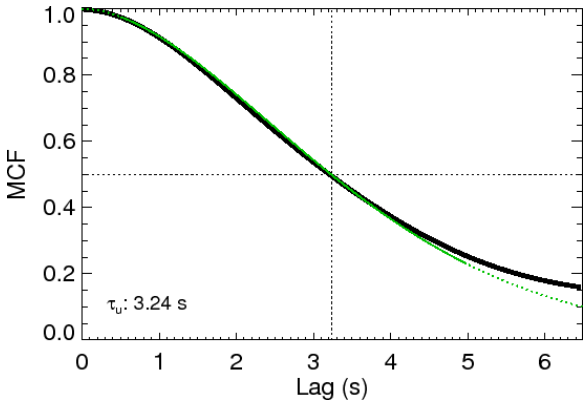

Figure 20. Mutual coherence function (black) computed from the intensity and phase measurements shown in Figure 18. The decorrelation time of the MCF is labeled. The fitted MCF is shown in green.

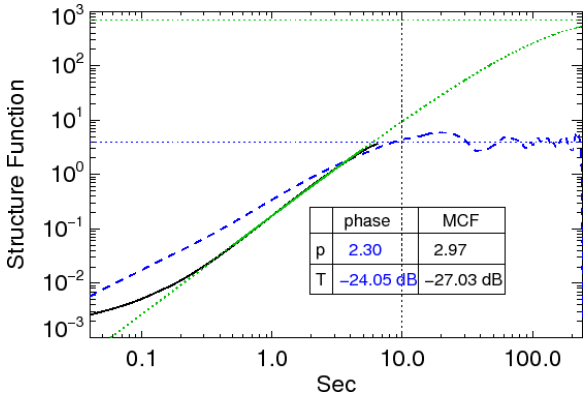

Figure 21. Structure function of screen phase (black) derived from the MCF shown in Figure 20. The fitted phase structure function is shown in green. Shown for comparison is the structure function of phase fluctuations at the ground (blue dashed).

5. CONCLUSIONS

In this study, we specify the conditions of the disturbed ionosphere using multiple phase screens and then forward-propagate the field to predict the values of phase spectral strength T and slope p that would be measured by a GNSS scintillation monitor

by fitting the spectral density function of phase fluctuations at the ground. We compare these results with those specified in the simulation to quantify the errors introduced by diffraction which accumulate as the radio wave propagates down to the ground.

Our simulation results show that the phase structure function derived from the mutual coherence function (MCF) is essentially that of path integrated phase, i.e. that due to an equivalent phase changing screen. The latter is most closely related to the irregularities that cause scintillation because it excludes the effects of diffraction. Leveraging this idea, we introduce an improved technique for estimating T and p by least-squares fitting the structure function of screen phase derived from the MCF using a statistical model. A quantitative comparison with known parameters of the simulation reveals these estimated parameters to be uncorrupted by diffraction effects.

We apply this fitting technique to GPS scintillation observations in Brazil and find the results to be very similar to the simulations. For this reason, we believe the fitting technique is effectively mitigating the effects of diffraction and accurately recovering the statistical parameters that describe the ionospheric irregularities from the scintillation measurements on the ground. Additional research needs to be conducted to determine whether the mutual coherence might vary within the medium in response to correlated structure along the propagation path.

This fitting technique is straightforward and suitable for implementation in the firmware of next-generation GNSS scintillation monitors to provide improved real-time characterization of ionospheric irregularities under both weak and strong scintillation conditions. We conclude by noting that accurate characterization of the irregularities also enables improved forward-propagation modeling of scintillation effects at frequencies and along ray-paths other than those actually measured.

AKNOWLEDGEMENTS

This research was supported by Boston College Cooperative Agreement FAA 11-G-006, sponsored by Deane Bunce.

REFERENCES

Carrano, C. S., Groves, K.M. (2010), Temporal Decorrelation of GPS Satellite Signals due to Multiple Scattering from Ionospheric Irregularities, Proceedings of the 23rd International Technical Meeting of The Satellite Division of the Institute of Navigation (ION GNSS 2010), Portland, OR, September 2010, pp. 361-374.

Carrano, C. S., K. M. Groves, R. G. Caton, C. L. Rino, and P. R. Straus (2011), Multiple phase screen modeling of ionospheric scintillation along radio occultation raypaths, Radio Sci., 46, RS0D07, doi:10.1029/2010RS004591.

Carrano, C. S., C. E. Valladares, and K. M. Groves (2012a), Latitudinal and local time variation of ionospheric turbulence parameters during the Conjugate Point Equatorial Experiment in Brazil, Int. Journal of Geophysics, vol. 2012, Article ID 103963, 16 pages, doi:10.1155/2012/103963.

Carrano, C. S., Groves, K. M., McNeil, W. J., Doherty, P. H. (2012b), Scintillation Characteristics Across the GPS Frequency Band, Proceedings of the 25th International Technical Meeting of The Satellite Division of the Institute of Navigation (ION GNSS 2012), Nashville, TN, September 2012, pp. 1972-1989.

Carrano, C. S., Groves, K. M., McNeil, W. J., Doherty, P. H. (2013), Direct Measurement of the Residual in the Ionosphere-Free Linear Combination during Scintillation, Proceedings of the 2013 International Technical Meeting of The Institute of Navigation, San Diego, California, January 2013, pp. 585-596.

Carrano, C. S., K. M. Groves, S. H. Delay, and P. H. Doherty (2014), An Inverse Diffraction Technique for Scaling Measurements of Ionospheric Scintillations on the GPS L1, L2, and L5 Carriers to Other Frequencies, Proceedings of the 2014 Institute of Navigation ION ITM meeting, San Diego, California, January 27-29, 2014.

Carrano, C. S., K. M. Groves, S. H. Delay, and P. H. Doherty (2015), A Novel Approach for Monitoring Zonal Irregularity Drift using a Stand-Alone GNSS

Scintillation Monitor, Proceedings of the 2015 International Technical Meeting of The Institute of Navigation, Dana Point, California, January 26-28, 2015.

Knepp, D. L. (1983), Multiple phase-screen calculation of the temporal behavior of stochastic waves, Proc. of the IEEE, 71, 6.

Nelder, J. and R. Mead (1965), A simplex method for function minimization", Computer Journal, 7, 749-756.

Rino, C. L. (1979), A power law phase screen model for ionospheric scintillation, 1. weak scatter, Radio Sci., 14, 1135-1145.

Rino, C. L., and J. Owen (1982), The mutual coherence function for transionospheric radiowaves, Rad. Sci., 17, 3, 675-683.

Welch, P. D. (1967), The use of fast Fourier transform for the estimation of power spectra: a method based on time averaging over short, modified periodograms, *IEEE trans. on Audio and Electroacoustics*, vol. au-15, no. 2.

Yeh, K. C., and C. H. Liu (1982), Radio wave scintillations in the ionosphere, Proc. IEEE, 70, 324–360.